EUROPEAN ORGANIZATION FOR NUCLEAR RESEARCH

PROPOSAL to the ISOLDE and Neutron Time-of-Flight Committee

Local Probing of Ferroic and Multiferroic Compounds

FERMULCOM -Collaboration

11th of January 2017

A.M.L. Lopes[1], J. Schell[2,3], V.S. Amaral[4], C.O.Amorim[4], J.P. Araújo[1], A. Baghizadeh[4], M. Baptista[1], Hans-Werner Becker[5], M. Escobar Castillo[3], J.G. Correia[6,2], A. Fenta[4], J.N. Gonçalves[4], H. Haas[4], M. Kachlik[7], S. Kamba[8], A. L. Kholkin[4], A.A. Lourenço[4], D. C. Lupascu[3], K. Maca[7], G. Oliveira[1], S. Picozzi[9], A.L. Pires[1] , E. C. Queirós[10], P. Rocha-Rodrigues[1], V. V. Shvartsman[3], M.R. Silva[6], A. Stroppa[9], P.B. Tavares[10], J.M. Vieira[4], Yulian Vysochanskii[11]

[1] *IFIMUP, Fac. Ciências, Univ. Porto, P-4150 Porto, Portugal*
[2] *European Organization for Nuclear Research (CERN), CH-1211 Geneva, Switzerland*
[3] *Institute for Materials Science and Center for Nanointegration, Duisburg-Essen (CENIDE), University of Duisburg-Essen, 45141 Essen, Germany*
[4] *Dep. Physics and CICECO, Univ. Aveiro, P-3810-193 Aveiro, Portugal*
[5] *Ruhr-Universität Bochum, RUBION, Universitätsstr. 150, D-44801 Bochum*
[6] *C²TN, Centro de Ciências e Tecnologias Nucleares, Instituto Superior Técnico, Universidade de Lisboa, Portugal*
[7] *CEITEC - Central European Institute of Technology, Brno University of Technology, Purkyňova 123, 612 00 Brno, Czech Republic*
[8] *Institute of Physics, Czech Academy of Sciences, Na Slovance 2, 182 21 Prague 8, Czech Republic*
[9] *CNR-SPIN 67100 L'Aquila, Italy*
[10] *Dep. Chemistry, UTAD, 5001-801 Vila Real, Portugal*
[11] *Institute of Solid State Physics and Chemistry, Uzhgorod University, Uzhgorod, Ukraine*

Spokespersons:
A.M.L. Lopes (Armandina.Lima.Lopes@cern.ch)
Juliana Schell (juliana.schell@cern.ch)

Local Contact:
J. G. Correia (Guilherme.Correia@cern.ch)

CERN-INTC-2017-020 / INTC-P-502
11/01/2017

Abstract

We propose to locally study, at the nanoscopic scale, materials that present ferroic (ferroelectric or magnetic) and multiferroic states, using the Perturbed Angular Correlation (PAC) radioactive nuclear technique. Our aim is to provide local and element selective information on some of the mechanisms that rule structural, charge, and orbital correlations, electronic and magnetic interactions, and the coupling of the associated degrees of freedom. The source of information is the study of the hyperfine magnetic and electric field gradient measured at different probe elements on a chosen set of flagship materials. The use of appropriate probe elements requires short-lived or radioactive elements specifically produced at ISOLDE and some long lived isotopes produced elsewhere to be implanted at RUBION-Bochum or BONIS-Bonn. All samples are measured at the ISOLDE PAC laboratories,

allowing systematic and detailed comprehensive studies, targeted at particular lattice sites of the samples. The overall study also comprehends the theoretical modeling of the systems (DFT *ab-initio*) and their characterization by conventional macroscopic techniques.

CASE STUDIES

PRIORITY CASES
2.1 Bismuth ferrite ($BiFeO_3$)
2.2 Silver niobate ($AgNbO_3$)
2.3 Magnetoelectric, Multiferroic Lu-Fe-O and $LuMnO_3$
2.4 Ca3(Mn/Ti)2O7 Ruddlesden-Popper compounds

TEST CASES
2.5 Copper indium thiophosphate ($CuInP_2S_6$)
2.6 Lead and Ba perovskite oxides ($PbTiO_3$, PbZrO3, $BaTiO_3$)
2.7 $ANiMnO_6$, A = In, Y, Bi Double perovskites

Requested shifts: 25+25 shifts, (for 2 years)

1 MOTIVATION & STRATEGY

The present work relies on an already long standing collaboration on material's research exploring complementarity of expertise and available techniques, now joining together to use the Perturbed Angular Correlation nuclear radioactive technique using short-lived / specific isotopes produced at ISOLDE- CERN. Long lived isotopes commercially available (^{111}In) or n-activated (^{181}Hf), to be measured at the ISOLDE PAC laboratories during the winter shutdown and off beam time periods will be implanted at RUBION-Bochum or BONIS-Bonn ion beam facilities. The proposed work follows the collaborative research methodology of the previous projects, such as IS390 and IS487, but the new working program is strengthened by the recognition of the possibilities brought by the complementary use of several short-lived probes produced at ISOLDE and also long-lived implanted at RUBION-Bochum and BONIS-Bonn. This allows for a more detailed and comprehensive study, targeted at particular crystal sites of the samples. It should be noted that in most cases the probe species (element) is a constituent of the sample under study or a substitutional impurity, which in principle simplifies the questions of its location and also the theoretical modelling of the hyperfine properties.

At ISOLDE, we will perform local studies to understand some of the relevant structural and charge mechanisms of the materials. γ–γ Perturbed Angular Correlation (PAC) probe local environments are determined via the electric field gradients (EFGs) and magnetic hyperfine field (MHF). These experiments allow for an atomic scale insight to the local structural deformations and charge/orbital distributions, validated by appropriate modelling. Moreover, the dynamic or static character of the environment can be examined. The radioactive isotopes will be implanted into pellets, single crystals, and thin films of these materials and the PAC studies will be performed after implantation and suitable annealing procedure. The measurements shall be done in a broad temperature range (10-1000K) to encompass the different ferroic phases with changes often linked to structural phase transitions.

The work at ISOLDE is complemented by electric and magnetic measurements and by a large variety of crystallographic techniques offered at the home laboratories. In particular, complementary temperature dependent X-ray diffraction and high-resolution transmission electron microscopy with electron diffraction are performed in the same samples. Highlights of our work are [OLI2012, GON2012, LOP2008].

The availability of beams of radioactive isotopes of a large variety of elements with high purity and yield makes the ISOLDE laboratory the unique facility where this interdisciplinary experimental program is envisaged and executed.

For each main subject we present the motivation and discuss the experimental program to be followed.

In recent years, multiferroic materials have been intensively studied to promote and understand the possibility of controlling magnetic properties by electric fields instead of magnetic fields which opens the path to faster, smaller, and more energy-efficient spintronic devices, such as memory elements, high-frequency magnetic devices, and micro-electro-mechanical systems, for data-storage technologies [FIE2016], [TOK2014], [TOK2014]. Many of the remarkable physical properties of multiferroics arise from the concomitant breaking of space-and time-inversion symmetries. The role of symmetry is thus of primary concern and its local probing becomes of particular interest. Moreover, a wealth of mechanisms, in addition to the displacive mechanism, were identified to promote spontaneous polar order. Particularly interesting is the case of improper ferroelectric materials (e.g. magnetically driven) which present domains and domain walls with properties and electronic functionalities that do not occur if the polarization is a primary order parameter.

In the large number of ferroic/multiferroic families, we propose first to study mostly materials which are being considered relevant to develop room-temperature applications, pure or with appropriate modifications and doping. Secondly, the availability of elements/isotopes and the modern instruments will be exploited for a comprehensive fundamental study of (simpler) materials, for which detailed theoretical modelling is available, usually using computer codes based on ab-initio density functional methods (DFT such as VASP and Wien2k).

Further one should also highlight the collaboration-added value possible at ISOLDE, joining material science researchers and students using different methods and complementary techniques. The desired high quality scientific outcome is accompanied by young people doing MSc and PhD thesis, who come here in many cases from outside of the nuclear world, for the first time encountering radio-isotopes, nuclear techniques, and nuclear-atomic interactions, the whole delivered on a true synergetic combination of efforts and results, a unique opportunity on people's training and careers.

2 CASE STUDIES

PRIORITY CASES

2.1 Bismuth ferrite ($BiFeO_3$)

Compared to other multiferroic materials bismuth ferrite, $BiFeO_3$, exhibits both ferroelectricity and antiferromagnetism at room temperature [SHI2016], enabling the construction of new multifunctional devices. It has a rhombohedrally distorted perovskite structure of space group R3c with high Neel T_n= 643 K and ferroelectric ordering T_c=1103 K temperatures [DAI2013]. Interestingly, these temperatures can vary subtly as a function of the particle size [LAN2014]. Whereas a spontaneous polarization in the [001]-axis is generated by Bi^{3+} and Fe^{3+} cations, the magnetic moments of Fe^{3+} cations presents a canted antiferromagnetic G type ordering. The small canting angle is caused by the magnetoelectric coupling to the polarization [LAN 2014]. The reason for the use of the PAC technique is due to its high sensitivity to detect hyperfine electromagnetic fields. This in particular at varying (also high) temperature as can be observed in Figure 1, where we show the first successful PAC spectra recently obtained after implantation of ^{181}Hf/Ta into $BiFeO_3$ pellets. We expect that combining PAC measurements using exotic and conventional probes such as ^{204}Bi/Pb, ^{111}In/Cd, ^{111m}Cd/Cd and ^{181}Hf/Ta may be optimal. The determination of the dielectric properties and the magnetic origin of ferroelectricity can be easier understood, if using inherent elements in the structure of the host material as nuclear probes. Eventually, studying $BiFeO_3$ when the probe interacts with point defects is interesting during the various phase transitions. In particular, one can possibly detect the antiferromagnetic ordering break at a localized defect. The ^{204}Bi/Pb appears in this context as an especially effective probe because of its high measuring spin (4+) providing multiple observable

frequencies per Electric Field Gradient (EFG) and, therefore, greater sensitivity to deviations from axial symmetry than other PAC isotopes [FRI2004].

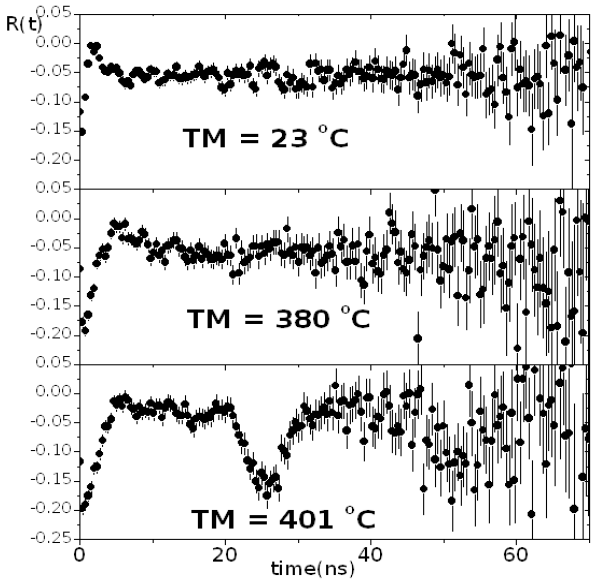

Figure 1: ^{181}Ta:$BiFeO_3$ γ-γ PAC decay from ^{181}Hf. The main clear frequency pattern that is observed is evidence for Ta occupying unique Bi sites in the lattice above the Neel temperature (T_N).

There the Ta atoms only see the characteristic lattice site EFG. At temperatures below T_N, the magnetic ordering sets in. But it orders in a cycloidal fashion across 65 nm. So every ion sees a different magnetic environment with respect to the electric field gradient, producing a distribution of fields that attenuate the PAC signal below T_N. There is now a full phenomenology of fields to be studied in detail down to 10 K.

This preliminary data shows the feasibility of the PAC technique and will be complemented with this proposal project and DFT simulations. While maintaining RUBION Perturbed Angular Correlation home laboratory, part of the research program will be done in parallel at ISOLDE in order to profit from the range of isotopes **only available at ISOLDE**. The cyclotron-produced ^{111}In(^{111}Cd) or reactor-produced ^{181}Hf(^{181}Ta) are common PAC probes that will be introduced into the samples via diffusion, implantation or chemistry processes at RUBION and cannot be produced frequently at ISOLDE.

2.2 Silver niobate ($AgNbO_3$)

Silver niobate is an attractive candidate for developing lead-free piezoelectric materials. The pure phase, $AgNbO_3$, exhibits ferroelectric behavior at room temperature, with a large polarization of 52 μC/cm^2 and a large electric field-induced strain under an electric field of 220 kV/cm [FU2007]. $AgNbO_3$ undergoes a complex sequence of phase transitions as a function of temperature and pressure. Above 852 K, $AgNbO_3$ is paraelectric, with a cubic (Pm•3m) symmetry. As temperature is lowered, it transforms sequentially to paraelectric tetragonal (P4/mbm) and orthorhombic (Cmcm) phases, followed by two antiferroelectric phases and one ferroelectric orthorhombic phase below 626 K [SCI2004, LEV2009]. The precise structures of antiferroelectric and ferroelectric phases are still matter of debates, with different space groups proposed by different research groups. So it was suggested that the atomic displacements are ordered in the ferrielectric way where the cation displacements are antiparallel to each other, but the associated dipole moments do not cancel each other completely resulting in a net spontaneous polarization along the c axis [YAS2011]. Moreover, there are two different Nb sites and three different Ag sites showing different displacement. The weak room temperature ferroelectric behavior was also attributed to local defects such as Ag vacancy clustering [SCI2004]. Levin et al. [LEV2009] also reported that the ferroelectric phase has a Pbcm symmetry and attributed its ferroelectricity to local cation displacement disorder. Recently, Yashima et al. [YAS2011] as well as [CHA2012] proposed space group Pmc21 for the ferroelectric phase based on the results of electron diffraction, neutron, and synchrotron powder diffraction experiments. Clarification of the different symmetries of the ferroelectric and antiferroelectric phases and their relative stabilities is an essential step in understanding the phase transition mechanisms in this system and should help promote the development of new and improved ferroelectric materials. D. Fu et al. proposed that the field induced ferroelectric state with large polarization originates from the transition of Ag ions to the ferroelectric arrangement [FU2007]. Li or K substitution at the Ag site also leads to

large polarization and piezoelectric responses [FU2008, FU2009]. Furthermore, $AgNbO_3$ has also attracted attention as a microwave material [VAL1999] and a visible-light responsive photocatalyst [KAT2002].

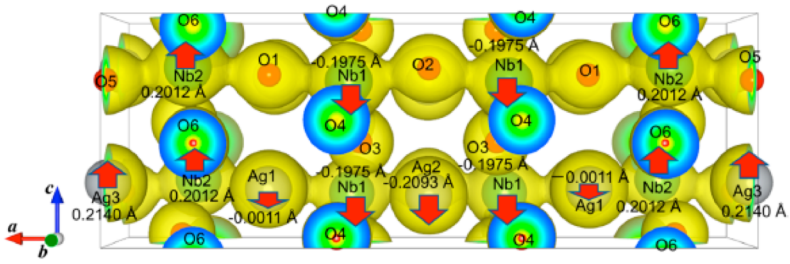

Figure 2: Electron-density distributions of low temperature ($Pmc2_1$) phase of $AgNbO_3$ obtained by density functional theory (DFT) calculations [YAS2012].

Taking into account the interest in experimentally learning about the particular role of the Ag^+ ion on the functional properties of $AgNbO_3$ [YAS2012] this is an ideal case study for PAC studies with the ^{111}Ag/Cd probe. The ceramic samples of pure $AgNbO_3$ and substituted systems like $Ag_{1-x}Li_xNbO_3$, $Ag_{1-x}K_xNbO_3$ are currently prepared at UDE (institution 3 of author list).

2.3 Magnetoelectric, Multiferroic Lu-Fe-O and $LuMnO_3$

The proposed work aims to explore four different phases of Lu-Fe-O ($LuFe_2O_4$, $LuFeO_3$, $Lu_2Fe_3O_7$ and $Lu_3Fe_5O_{12}$). Lu-Fe-O system [SEK1976] is the first iron based single-phase multiferroic system in which both the magnetisation and electric polarization are associated to the iron sites and with strong iron-iron correlations, leading to the appealing observation, in bulk $LuFe_2O_4$ system, of a large change in magnetization induced by applying electrical pulses [LI2009].

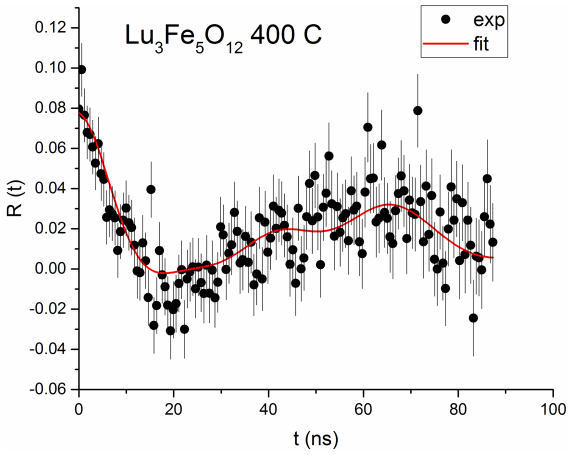

Figure 3: Test PAC measurement with implanted ^{111m}Cd in a garnet $Lu_3Fe_50_{12}$ sample measured at 400 ºC (673 K). The perturbation function may be related to one local environment by the preliminary fit, which corresponds to a V_{zz}=5.4 10^{21} V m^{-2}, and η=0.4.

In spinel $LuFe_2O_4$, iron based charge order (CO) is coupled with the spin degree of freedom [ZHA2007]. Three-dimensional (3D) CO exist up to 320 K and two-dimensional (2D) ferrimagnetic ordering up to 240 K [ROU2010]. Perovskite $LuFeO_3$ phase crystallizes in orthorhombic (o-$LuFeO_3$) or hexagonal (h-$LuFeO_3$) structures. O-$LuFeO_3$ is stable in bulk with antiferromagnetic nature but not ferroelectric. Obtained in thin film, h-$LuFeO_3$ is ferroelectric up to 1050 K and weak ferromagnetism up to 440 K was found, therefore multiferroic at room temperature [WAN2013]. This result was however contrasted by more recent studies [DIS2015]. Nevertheless, morphotropic phase coexistence was fond [SON2016]. Sc doping [DIS2015b] and heterostructure growth [MUN2016] have led to a controlled increase of multiferroism temperature range up to room temperature, stabilizing the h-phase.

The intercalation of $LuFeO_3$ single layer between two $LuFe_2O_4$ double layers i.e., the compound $Lu_2Fe_3O_7$, is another effective approach to tune the dielectric properties and magnetism [MA2012], leading to a Neel temperature of 255 K [TAN1983] and remarkable multiferroic nature in correlation with the essential charge order. Further, $Lu_3Fe_5O_{12}$, a Rare-Earth Iron Garnet, exhibits an interesting low field magneto-dielectric response at room temperature [WU2009, MAN2015]. However, $Lu_3Fe_5O_{12}$ does not possess spontaneous polarization or satisfy the symmetry constrains for linear ME effect observed in other three phases of Lu-Fe-O system. Heterostructures appear thus as a promising

route to enhance and exploit multifunctional effects at room temperature, and the guidance of nanoscopic characterization is of considerable interest.

It should be noted that, similar to hexagonal manganite $LuMnO_3$, its electric polarization tracks the Lu-trimer distortions [DAS2014]. PAC experiments will also be performed in the similar $LuMnO_3$ hexagonal phase material, for what we present already some proof – of – concept work perform with test experiments using the ^{111m}Cd/Cd PAC probe.

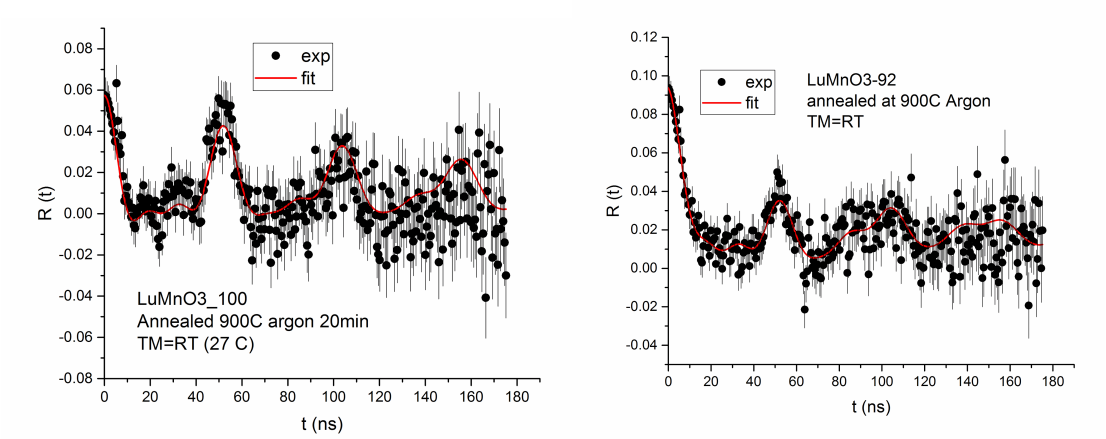

Figure 4 (left): Test PAC experiments performed with ^{111m}Cd implanted PAC spectrum in Stoichiometric $LuMnO_3$ at room temperature. The fit shows one local environment with an EFG of V_{zz}=8.0 10^{21} V m^{-2}, η=0.15; **(right)** ^{111m}Cd implanted PAC spectrum in Mn-poor (x_{Mn}=0.92) $LuMnO_3$. The fit shows two local environments with EFG1 V_{zz}=7.9 10^{21} V m^{-2}, η=0.24, and EFG2 V_{zz}=3.4 10^{21} V m^{-2}, η=0.

2.4 $Ca_3(Mn/Ti)_2O_7$ Ruddlesden-Popper compounds

Naturally Layered Multiferroics offer an inspiring route towards less expensive and high performance room temperature magnetoelectric coupling. In these systems electric polarization is not the primary order parameter at the phase transition, being induced by the coupling of two or more non-polar lattice instabilities, e.g., BO6 octahedra rotations at adjacent perovskite-like layers creating the hybrid improper ferroelectricity (HIF) [BEN2011]. Their potentialities, yet not explored, rely on the idea that ferromagnetism and ferroelectricity are coupled by the same lattice instability thus providing an indirect but strong magnetoelectric effect.

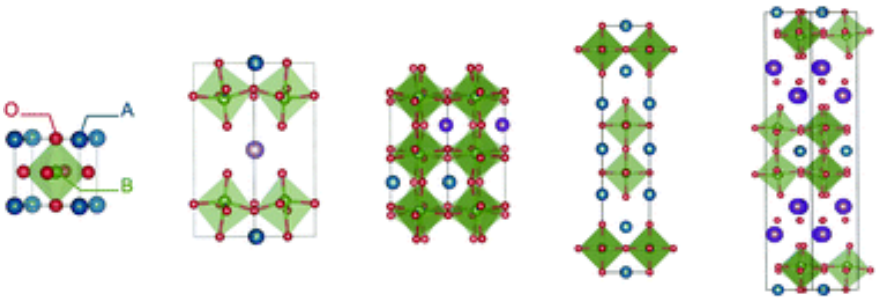

ABO_3 Cubic Perovskite	$A'[A_{n-1}B_n]O3_{n+1}$ Dion–Jacobson phases	Double perovskite $A'AB_2O_6$	Ruddlesden-Popper $A_{n+1}BnO3n+1$	$Bi_2O_2[A_{n-1}BnO_{3n+1}]$ Aurivillius phases

Figure 5: Layered perovskites[BEN2015].

Octahedra distortions in a simple perovskite are usually non-polar but the discovery of polarization in artificial SrTiO3/PbTiO3 [BOU2008] by the coupling of two rotation modes inspired the search for polarization in naturally layered perovskite-like structures (NLP) such as Ruddlesden-Popper [OH2015], Double Perovskites [SAG2014], and Aurivillius phases [YUA2015]. Though many systems were already proposed, experimental confirmations are rare. This lack of evidence arises essentially due twofold type of reasons: -high electric leakage currents that might lead to

unrepresentative features of the intrinsic properties of the material -properties arising from local structural features that are not well described by a crystallographic approach based on long-range average models.

Thus a thorough local scale examination in promising perovskite-like layered structures chasing local distortions/instabilities is mandatory, such as obtained using Perturbed Angular Correlations.

The idea of using Ruddlesden-Popper (RP) series $A_{n+1}BnO_{3n+1}$ as scaffolds for strong MEs is not entirely new but the theoretical grounds for hybrid improper ferroelectricity [BEN2011], its experimental demonstration [OH2015] and $(Ca,Sr)_3Ti_2O_7$ domain topology just appeared [HUA2016]. Nevertheless, first-principles calculations predicted that these compounds have too high energy barriers for polarization switching [MUL2013] and thus to foreseen any practical application it is also necessary to circumvent this problem by finding a set of pathways to raise polarization while keeping low energy barriers. This might be feasible though appropriate site substitution [PIT2015] . In these systems polarization can also be controlled by strain. In fact, a strain-induced polar-to-nonpolar transition with a critical tensile strain beyond which the polar nature suddenly turns off was just claimed in Ca3(Mn,Ti)2O7 and Sr3 Zr2 O7 thin films [LU2016].

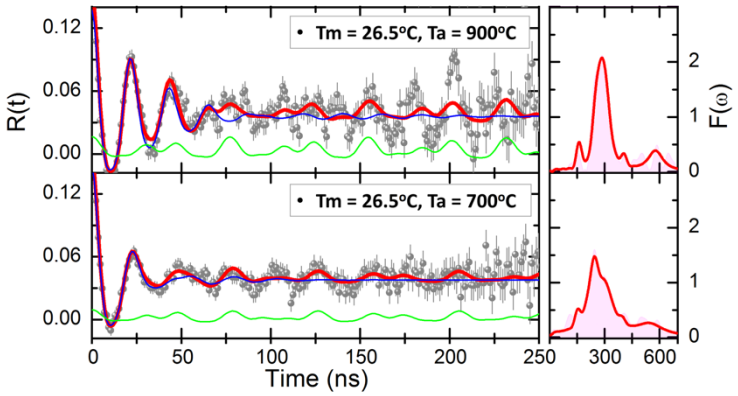

Figure 6: Layered Comparison of (R(t)-function) for the $Ca_3Mn_2O_7$ compound, for the two distinct annealing temperatures of 900ºC (top) and 700ºC (bottom); measuring PAC at room temperature.

Well above room temperature the $Ca_3(Mn,Ti)_2O_7$ crystal structure is predicted to be tetragonal, space group I4/mmm, and orthorhombic A21am at the low temperature ferroelectric phase. Nevertheless, based on the Landau theory of phase transitions a direct transition from I4/mmm to A21am is not allowed and it is referred that the transition should proceed via an intermediate phase. Up to now no such intermediate phase has been observed. Instead, in $Ca_3Mn_2O_7$, a complex phase competition over a large temperature range and a "symmetry trapping" of a soft mode leading to a large uniaxial negative thermal expansion was recently observed [SEN2015]. The symmetry details, compatibility with a HIF phase transition and transition temperatures $Ca_3(Mn,Ti)_2O_7$ are still under great debate. Moreover, no direct evidence for existence of HIF has been reported in $Ca_3Mn_2O_7$, making this an appealing system to search an improved local scale understanding.

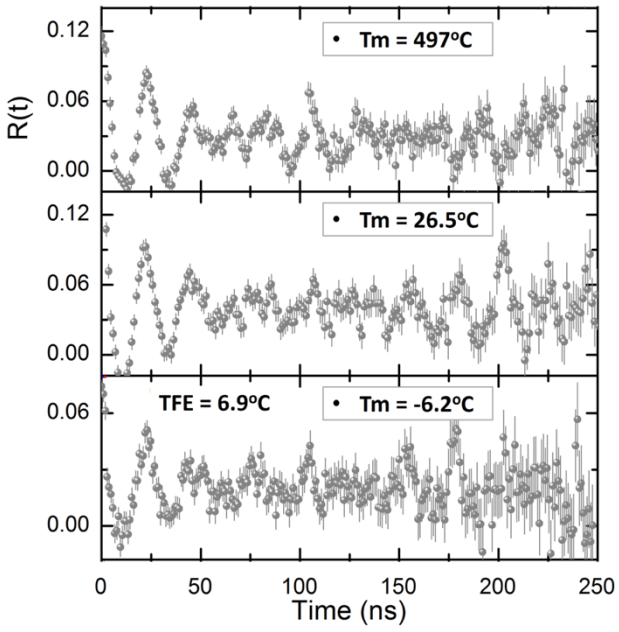

Figure 7: R(t)-function for the $Ca_3Mn_2O_7$ compound, for three distinct measuring temperatures of 497ºC (tetragonal I4/mmm); 26.5ºC (orthorhombic); -6ºC (Ferroelectric, orthorhombic).

Preliminary experimental work was already undertook targeting specifically the RP phase $Ca_3(Mn_{1-x}Ti_x)_2O_7$ series, starting with low Ti doping in the $Ca_3Mn_2O_7$ parent compound (x = 0, 0.1, 0.2). PAC measurements were performed in home-made ceramics at the CERN-ISOLDE facilities using the ^{111m}Cd probe. First, we found

that to minimize the crystal's lattice defects created by the ion implantation a annealing in air at 900ºC (and 20 min duration) is the most suitable for this class of materials.

Measurements were then performed on those three samples in the temperature range from 497 ºC down to -6ºC. A well-defined R(t)-function for the distinct phases of the compound $Ca_3Mn_2O_7$ was observed proving the feasibility of the measurements.

TEST CASES

2.5 Copper indium thiophosphate ($CuInP_2S_6$)

$CuInP_2S_6$ crystals represent an example of an anti-collinear two-sublattice ferrielectric system. It shows a first-order phase transition of order-disorder type from the paraelectric *(C2/c)* to the ferrielectric (*Cc*) phase (*Tc* = 315 K). The symmetry reduction occurs due to ordering in the copper sublattice and displacement of cations in the indium sublattice from their centrosymmetric positions. Shifts of Cu^+ and I^{3+} ions are antiparallel, but have different magnitude. The arising ferroelectric spontaneous polarization is perpendicular to the layer planes [BEL2015]. These thiophosphates consist of lamellae defined by a Sulphur framework, in which the metal cations and P-P pairs fill the octahedral voids; the Cu, In, and P-P ions form triangular patterns within the layer. The cation off-centering, 1.6 for Cu^+ and 0.2 Å for In^{3+}, may be attributed to a second order Jahn-Teller instability associated with the d^{10} electronic configuration [DZI2012]. The lamellar matrix absorbs the structural deformations via the flexible P_2S_6 groups while restricting the cations to antiparallel displacements that minimize the energy cost of dipolar ordering. Each Cu ion can occupy two different positions. A coupling between P_2S_6 deformation modes and Cu^+ vibrations enables the copper ion hopping motions that lead to the loss of polarity and the onset of ionic conductivity in this material at higher temperatures [KLE2011]. A similar compound is $CuCrP_2S_6$. It undergoes a first-order phase transition into an antiferroelectric *(C2/c)* phase at 150 K. At 190 K this compound undergoes a second-order phase transition from the paraelectric (to a quasi-antiferroelectric (incommensurate) phase. In this intermediate phase incomplete antipolar ordering of the copper was found. Besides, below T_N = 32 K the material shows an antiferromagnetic order. So $CuCrP_2S_6$ can be considered as an multiantiferroic. $CuInP_2S_6$ and $CuCrP_2S_6$ form solid solutions. For the $Cu_{0.8}In_{0.2}CrP_2S_6$ a magnetoelectric effect was measured. Therefore, PAC studies using ^{111}In/Cd, ^{111m}Cd/Cd are envisaged on $CuInP_2S_6$ probing the In site. The fact that upon decay In becomes a Cd atom where PAC actually performs the measurement can induce delayed, ns, electronic excitations, which do not happen when using the ^{111m}Cd/Cd probe that acts as a countercheck for that event. In the case of a slow electronic recovery, that permits studying locally an electronic doping effect and its characteristic time recombination as a function of temperature, a local measurement of electron mobility on the material is provided. Actually, the

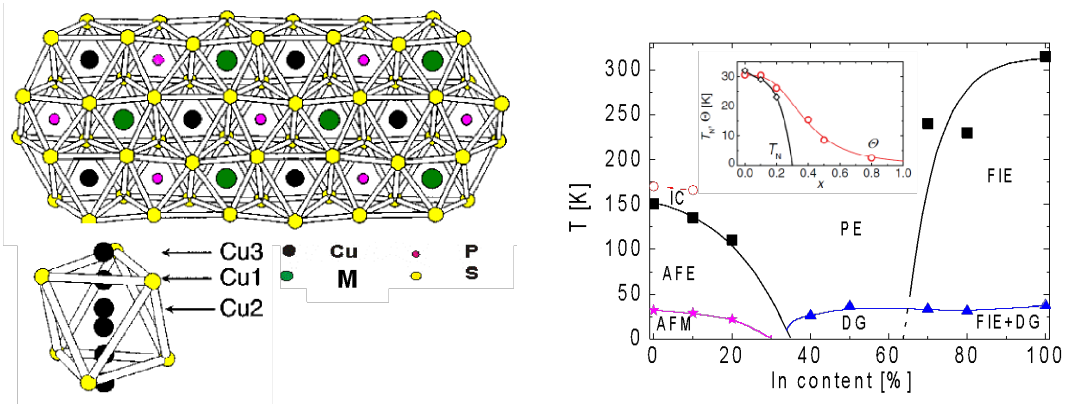

Figure 8 (left): Structure of thiophosphates $CuMP_2S_6$; **(right)** Phase diagram of $CuIn_xCr_{1-x}P_2S_6$ crystals, from [DZI2012]. The inset shows the magnetic phase diagram [KLE2011].

system can be further tested with the PAC probe ^{117}Ag(73s)→ ^{117}Cd(2.4h)→^{117}In that can be easily obtained during Ag beam times. Two ideal isotopes can be envisaged to get more insight into this

material that would be object of a different proposal, ^{68m}Cu(3.75min)/Cu and ^{48}Cr(21.5h)/V, the first requiring on-line experiments, the second requiring further development of target / ion sources at ISOLDE.

The samples are obtained from Prof. Y. Vysochanskii, Institute of Solid State Physics and Chemistry, Uzhgorod University, Uzhgorod, Ukraine or from Prof. J. Banys, Faculty of Physics, Vilnius University, Vilnius, Lithuania.

2.6 Lead and Ba perovskite oxides ($PbTiO_3$, $PbZrO_3$, $BaTiO_3$)

$PbTiO_3$ is a much studied ferroelectric, with large values of polarization and a tetragonal ferroelectric phase at room temperature which transits to a cubic paralectric phase above the Curie point. Related systems are used in applications, especially in the mixed system form such as $PbZrO_3$–$PbTiO_3$ (PZT) with a morphotropic phase boundary separating different phases [KUW1981], where high piezoelectric coefficients are found. With regard to the mixed systems, there have been PAC studies with the ^{181}Ta probe, in PZT [GUA2007] near the morphotropic phase boundary, and also in $PbTi_{1-x}Hf_xO_3$ at different concentrations including the ferroelectric and paraelectric phases [ALO2012]. However, the prototypical ferroelectric $PbTiO_3$ has been studied by perturbed angular correlation spectroscopy (PAC) only using the $^{181}Hf \rightarrow {}^{181}Ta$ probe, which is supposed to occupy the Ti site, and an electric field gradient (EFG) was obtained [CAT1996]. The cubic paraelectric to tetragonal ferroelectric phase transition was studied. An interval of coexistence was found, and one could fit a power law to the critical region. The obtained EFG changes were weak and the accuracy of this fit could be improved.

There were two reports using the Pb PAC probe, which showed a narrow distribution with $\eta \approx 0$ for PbTiO3 [HER1974], as expected, and the other which confirmed the previous value [DIE2003], as well as one in the PZT system near the MPB [DIE2003].

Using density functional theory calculations, we have previously demonstrated that the EFG should be especially sensitive to spontaneous polarization variations, following a general systematic, nearly quadratic trend. However, with increasing sensitivity at the A-site with increasing atomic number it is strongest when Pb is present [GON2012]. It would then be of interest to study the phase transition, to complement the previous PAC study, as well as the general temperature variation, at the Pb site, in order to get the EFG(P) relationship calculated in the previous theoretical study, as shown in the figure.

We have also shown, comparing the A-sites of different materials with $BaTiO_3$-like distortions, that when Pb is the A site the coefficient of proportionality between EFG and polarization is larger, as shown in the next figure, with $PbZrO_3$ as the example, which is the other end compound of the PZT system. Therefore, we intend to extend the hyperfine study also to $PbZrO_3$ and $BaTiO_3$ materials.

With the Pb PAC probe isotopes this experiment is especially interesting since we avoid the general PAC interpretation problems occurring when the probe is not an element in the host material. The results should be simpler and easier to interpret, and the probes should go to the corresponding Pb sites in the host.

Calculations in PZT in the different phases (tetragonal, monoclinic, rhombohedral) have also shown that the Pb site is more sensitive to EFG changes [MAO2007], and diffraction measurements show polarization density at the Pb site [TAN2006].

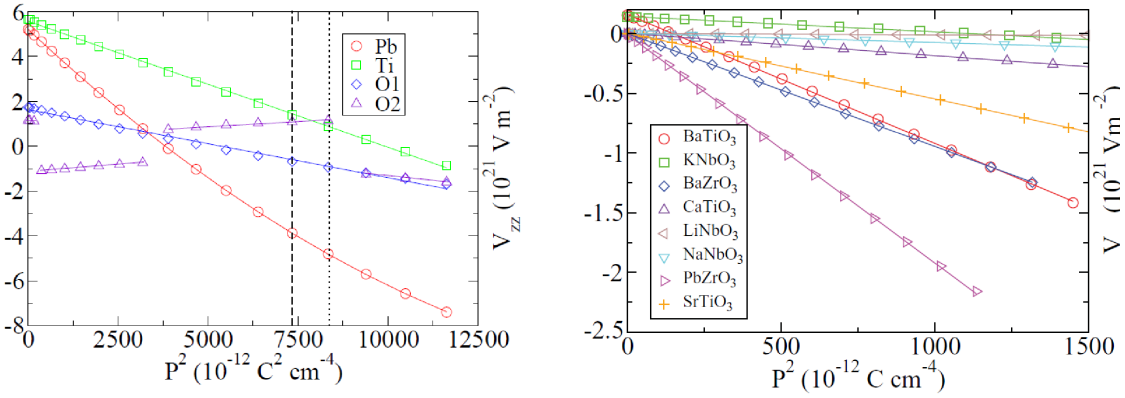

Figure 9 (left): V_{zz} as a function of the polarization squared in the tetragonal ferroelectric phase of $PbTiO_3$ [GON2012]; **(Righ)** V_{zz} as a function of the polarization squared in the tetragonal ferroelectric phases with distortions like $BaTiO_3$, for the materials shown in the legend.

The accurate measurement of the EFG is also important, as well as its calculation, to compare with other theoretical approaches, and given its possible importance in the possible detection of violations of PT symmetries due to the posited nuclear Schiff moment of the Pb nuclei [SKR2016] looking for the upper limit of the dipolar electric moment of the electron.

2.7 $ANiMnO_6$, A = In, Y, Bi Double perovskites

Hybrid improper ferroelectricity should also be commonly observed in the A-site ordered superlattices built from different ABO3 perovskites blocks, neither of which ferroelectric, since oxygen octahedron rotations are typical in these materials [BEN2015]. However, up to now only a few cases were experimentally confirmed to be polar (for example, NaLaMnWO6, which exhibits simultaneous A- and B-site cation ordering) [FUK2011].

In these layered perovskites one particularly well-studied case is the 50:50 substitution with the 3d metals at B site, as it tendentially leads to ferromagnetic order near room temperature. The Curie temperature is controlled by B-O-B' bond angle that can be tuned by changing the A site radius. For example, La2NiMnO6 demonstrates a ferromagnetic order at 280K (though not presenting a polar order). Nevertheless, the recently synthesized Bi2NiMnO6 double perovskite was found to be ferroelectric below 485K and ferromagnetic below 140K [AZU2005]. While this latter ordering occurs below room temperature efforts have been made to tailor the double perovskite, in such a way, that the interaction between the B-B' ions would promote the room temperature FM ordering and the A-sites ions would couple with ferroelectric ordering [ZHA2015] .

In those attempts a double perovskite Y2NiMnO6 was synthesized with different methods presenting a FM order below room temperature and a polarization of about 40 μC/m2 . The ferroelectric transition temperature is yet not consensual [ZHA2014]. Similarly, a weak FM multiferroic In2NiMnO6, with the In3+ at the A site, showed a ferroelectric polarization of 30 μC/m2 developing below room temperature [TER2015].

We propose to study the ANiMnO6 series with A = In, Y, Bi suitable chosen to correspond to local probe ions or similar. With its FM order, this series for which studies are scarce is technologically very appealing as most multiferroics are AFM. An improved local scale understanding, obtained through a thorough PAC study, will indubitably contribute to a comprehensive knowledge of these systems and guidance on the search for attractive characteristics.

3 Beam Time Request

NOTE: At the Appendices a resumed / detailed explanation of targeted thematic studies and working procedures are presented, from where we establish the present beam time request.

ISOLDE Beam	Approximate intensity (ion/μC of p-beam)	Target	Ion source	SHIFTS 1 + 1 years	Machine days per year	COMMENT
^{111m}Cd (49 m)	1 . 10^8	Molten Sn	Vadis MK5	12+12	4	(1), (2)
^{111}Ag (7.45 d)	10^9	UC2	RILIS	2 + 2	2/3	(3)
^{149}Gd (9.3d)	3. 10^9	UC2	Surface ioniser	1 + 1	1/3	(3)
^{172}Lu (6.7d)	2 . 10^7	Ta foil	Surface ioniser	2 + 2	2/3	(3)(4)
^{204m}Pb (67m)	5 . 10^7	UC2	RILIS	6 + 6	2	(1)(5)
^{204}Bi (11.2h)	1 . 10^7	UC2	RILIS	2 + 2	2/3	(3)(6)
			TOTAL (two years)=	25 + 25		

(1) The number of shifts reflect the necessity of a continued period of beam to build systematics on the same type, same batch of samples, when using short lived isotopes measured off-line (detailed procedure presented at Appendix A3). 12 shifts /year cover a 4 days' period of beam. With a Cycle of Preparation and Measurements (CPM) (Appendix A3) of 4-5 hours per sample about 5, e.g. temperature points can be, realistically, obtained per day. Each type of material (composition or doping) can only be measured on one PAC setup for measurements above RT and on another one for measurements below RT, avoiding systematic differences (Appendix A3). During a 4 days run, realistically we can expect obtaining ~20 measurements, as a function of temperature per machine. There are two PAC spectrometers measuring high temperature and two spectrometers measuring low temperatures. The proper characterization of a phase transition requiring 10 – 15 points, depending of the complexity and phenomenology under study. Therefore, between 4 and 8 different type of samples, allowing characterizing (composition) and temperature effects across the phase transitions could be envisaged to be studied on a four days run.

(2) We stress that the key issue for these PAC runs is the number of days in continuity more than the number of individual shifts since only a relatively small fraction of the isotope separator time is used, 20 – 40 min every 4h preparations and measurement time. Optimization with other groups requiring the same isotope is therefore a must. During these beam times the 6 PAC setups are assigned to the different users, and everyone gains from an extend beam time period, summing up all shifts; in other words, a 6 days run summing up shifts contribution from all approved experiments, working in parallel, is the ideal running way for all research projects.

(3) For long lived isotopes all samples are implanted on a batch to be measured afterwards. The measuring time is not accounted on requested beam time shifts, like in the case of short lived isotopes. These beam times must/can be scheduled with other (main) users of the same target / ion source.

(4) ^{172}Lu is presently best made at the end run of an "old" target. Then one can heat the line much more and gain significantly in yield and from the accumulation of Lu on the target. RILIS would definitively be better but no RILIS schema for Lu will be developed between now and end of 2018.

(5) ^{204m}Pb(67min) needs RILIS to avoid high activity from ^{204}Po(3.5h) and alpha recoils from ^{204}Rn(1.2min)→ ^{200}Po (11.5 min)→ … few day half-life contaminants.

(6) Preferentially done by RILIS, ^{204}Bi could also be made from surface ionized ^{208}Fr. 92% of this ends up in ^{204}Bi(11.2h), 4% in ^{208}Po (2.9y) and 4% in ^{200}Pb(21.5h)→^{200}Tl(26.1h)→^{200}Hg(stable).

References

[ALO2012] R. E. Alonso et al., Perturbed angular correlation study of 181Ta-doped PbTi1−xHfxO3 compounds, Physica B 407 2610–2616 (2012) http://dx.doi.org/10.1016/j.physb.2012.04.005

[AZU2005] M. Azuma, et al., Designed Ferromagnetic, Ferroelectric Bi2NiMnO6, J. Am. Chem. Soc. 127, 8889–8892 (2005); http://dx.doi.org/ 10.1021/ja0512576

[BEL2015] A. Belianinov et al., Spatially Resolved Probing of Electrochemical Reactions via Energy Discovery Platforms, Nanoletters 15, 3808-3814 (2015); http://dx.doi.org/10.1021/acs.nanolett.5b01613

[BEN2011] N. A. Benedek, et al., Hybrid Improper Ferroelectricity: A Mechanism for Controllable Polarization-Magnetization Coupling, Phys. Rev. Lett. 106(10), 107204 (2011); https://doi.org/10.1103/PhysRevLett.106.107204

[BEN2015] N. A. Benedek., et al., Understanding ferroelectricity in layered perovskites: new ideas and insights from theory and experiments, Dalton Trans. 44, 10543-10558 (2015); http://dx.doi.org/10.1039/c5dt00010f

[BOU2008] E. Bousquet, et al., Improper ferroelectricity in perovskite oxide artificial superlattices, Nature, 452 (7188), 732 (2008); http://dx.doi.org/10.1038/nature06817

[CAT1996] G. L. Catchen et al., Characterizing Phase Transitions in the Perovskites PbTiO3 and BaTiO3 Using Perturbed-Angular-Correlation Spectroscopy, Zeitschrift für Naturforschung A 51 411 (1996) http://zfn.mpdl.mpg.de/data/Reihe_A/51/ZNA-1996-51a-0411.pdf

[CHA2012] H. Chang et al. Hydrothermal Syntheses and Structural Phase Transitions of AgNbO3, J. Am. Ceram. Soc. 95, 3673 (2012). https://doi.org/10.1111/j.1551-2916.2012.05392.x

[DAI2013] H.Y. Dai, et al., Structural and Electrical Properties of Bismuth Ferrite Ceramics Sintered in Different Atmospheres, J. Supercond. Nov. Magn. 26, 3125–3132 (2013); http://dx.doi.org/10.1007/s10948-013-2130-7

[DAS2014] H. Das et al., Bulk magnetoelectricity in the hexagonal manganites and ferrites, Nature Communications 5, 2998 (2014); http://dx.doi.org/10.1038/ncomms3998

[DIE2003] M. Dietrich; talk presented at the ISOLDE/CERN Physics Workshop, Geneva, Switzerland, 15–17 December 2003; https://dl.dropboxusercontent.com/u/5987560/Hyperfine_Ferroelectric_Dietrich.pdf

[DIS2015] S. M. Disseler, et al., Magnetic Structure and Ordering of Multiferroic Hexagonal LuFeO3, Phys. Rev. Lett. 114, 217602 (2015) http://dx.doi.org/10.1103/PhysRevLett.114.217602

[DIS2015b] S.M. Disseler et al., Multiferroicity in doped hexagonal LuFeO3, Phys. Rev. B 92, 054435 (2015); http://dx.doi.org/10.1103/PhysRevB.92.054435

[DON2015] S. Dong, et al, Multiferroic materials and magnetoelectric physics: symmetry, entanglement, excitation, and topology, Advances in Physics, 64(5-6), 519-626 (2015) http://dx.doi.org/10.1080/00018732.2015.1114338

[DZI2012] A. Dziaugys et al., Phase diagram of mixed Cu(InxCr1−x)P2S6 crystals, Phys. Rev. B 85, 134105 (2012); https://doi.org/10.1103/PhysRevB.85.134105

[FIE2016] M. Fiebig, et al, The evolution of multiferroics, Nature Reviews Materials, 1, 16046 (2016) http://dx.doi.org/10.1038/natrevmats.2016.46

[FRI2004] S. Friedemann, et al., The Nuclear Quadrupole Interaction of 204mPb in Lead Oxides, Hyp. Interac. 159, 313 (2004); http://dx.doi.org/10.1007/s10751-005-9121-4.

[FU2007] D. Fu et al. On the phase identity and its thermal evolution of lead free (Bi1/2Na1/2)TiO3-6 mol% BaTiO3, APL 90, 252907 (2007); http://dx.doi.org/10.1063/1.3645054

[FU2008] D. Fu et al. Piezoelectric properties of lithium modified silver niobate perovskite single crystals, Appl. Phys. Lett. 92, 172905 (2008); http://dx.doi.org/10.1063/1.2918837

[FU2009] D. Fu et al. Dielectric, ferroelectric, and piezoelectric behaviors of AgNbO3–KNbO3 solid solution, J. Appl. Phys. 106, 104104 (2009); http://dx.doi.org/10.1063/1.3259410

[FUK2011] T. Fukushima, et al., Large ferroelectric polarization in the new double perovskite NaLaMnWO6 induced by non-polar instabilities, Phys Chem Chem Phys 13, 12186 (2011) http://dx.doi.org/10.1039/C1CP20626E

[GON2012] J. N. Gonçalves et al., Ab initio study of the relation between electric polarization and electric field gradients in ferroelectrics, Physical Review B 86, 035145 (2012) http://dx.doi.org/10.1103/PhysRevB.86.035145

[GUA2007] C. A. Guarany et al., Hyperfine interaction measurements on ceramics: PZT revisited, Physica B 389 130–134 (2007) http://dx.doi.org/10.1016/j.physb.2006.07.039

[HER1974] P. Herzog et al., Static electric quadrupole interaction of Ce and Pb ions in lead titanate; Z. Physik 269, 265–267 (1974). http://dx.doi.org/10.1007/BF01668692

[HUA2016] F.T. Huang et al., Domain topology and domain switching kinetics in a hybrid improper ferroelectric, Nature Commun. 7, 11602 (2016); http://dx.doi.org/10.1038/ncomms11602

[KAT2002] H. Kato et al. Role of Ag+ in the Band Structures and Photocatalytic Properties of AgMO3 (M: Ta and Nb) with the Perovskite Structure, J. Phys. Chem. B 106, 12441 (2002); http://dx.doi.org/10.1021/jp025974n

[KLE2011] W. Kleemann et al., Magnetic and polar phases and dynamical clustering in multiferroic layered solid solutions CuCr1−xInxP2S, Phys. Rev. B 84, 094411 (2011); http://dx.doi.org/10.1103/PhysRevB.84.094411

[KUW1981] J. Kuwata et al., Phase transitions in the Pb (Zn1/3Nb2/3)O3-PbTiO3 system, Ferroelectrics 37, 579 (1981); http://dx.doi.org/10.1080/00150198108223490

[LAN2014] J. Landers, et al., Mössbauer Study of Temperature-Dependent Cycloidal Ordering in BiFeO3 Nanoparticles, Nano Lett.14(11), 6061-5 (2014); http://dx.doi.org/10.1021/nl5031375

[LEV2009] I. Levin et al. The electric field induced ferroelectric phase transition of AgNbO3, Phys. Rev. B 79, 104113 (2009); http://dx.doi.org/10.1063/1.4941319

[LI2009] C-H. Li et al., Electrical control of magnetization in charge-ordered multiferroic LuFe2O, Phys. Rev. B 79, 172412 (2009); http://dx.doi.org/10.1103/PhysRevB.79.172412

[LOP2008] A.M.L. Lopes et al., New phase transition in the Pr1-xCaxMnO3 system: Evidence for electrical polarization in charge ordered manganites, Physical Review Letters 100, 155702 (2008) https://doi.org/10.1103/PhysRevLett.100.155702

[LU2016] X.-Z.Lu et al., Epitaxial-strain-induced polar-to-nonpolar transitions in layered oxides, Nature Mat. 15, 951 (2016); http://dx.doi.org/10.1038/nmat4664

[MA2012] C. Ma et al., Microstructure and oxidation states in multiferroic Lu2(Fe,Mn)3O7, J. Appl. Phys. 112, 094105 (2012); http://dx.doi.org/10.1063/1.4764309

[MAN2015] P. Manimuthu et al., Observation of direct magneto-dielectric behaviour in Lu3Fe5O12−δ above room-temperature, Phys.Chem.Chem.Phys.17, 17688 (2015); http://dx.doi.org/10.1039/c5cp02719e

[MAO2007] D. Mao et al., Structural dependence of electric field gradients in Pb(Zr1−xTix)O3 from first principles, Phys. Rev. B 76, 14105 (2007). https://doi.org/10.1103/PhysRevB.76.014105

[MUL2013] A.T. Mulder et al., Turning ABO3 Antiferroelectrics into Ferroelectrics: Design Rules for Practical Rotation-Driven Ferroelectricity in Double Perovskites and A3B2O7 Ruddlesden-Popper Compounds, Adv. Funct. Mat., 23 (38), 4810 (2013); http://dx.doi.org/10.1002/adfm.201300210

[MUN2016] J.A. Mundy et al., Atomically engineered ferroic layers yield a room-temperature magnetoelectric multiferroic, Nature 537, 523–527 (2016); http://dx.doi.org/10.1038/nature19343

[OH2015] Y. S. Oh et al., Experimental demonstration of hybrid improper ferroelectricity and the presence of abundant charged walls in (Ca,Sr)3Ti2O7 crystals, Nature Mat. 14, 407 (2015); http://dx.doi.org/10.1038/nmat4168

[OLI2012] G.N.P. Oliveira et al, Dynamic off-centering of Cr3+ ions and short-range magneto-electric clusters in CdCr2S4, Physical Review B 86, 224418 (2012) https://doi.org/10.1103/PhysRevB.86.224418

[PIT2015] M.J. Pitcher et al., Tilt engineering of spontaneous polarization and magnetization above 300 K in a bulk layered perovskite, Science 347, 420 (2015); http://dx.doi.org/10.1126/science.1262118

[ROU2010] J. Rouquette et al., Pressure-Induced Structural Transition in LuFe2O4: Towards a New Charge Ordered State, Phys. Rev. Lett. 105, 237203 (2010); http://dx.doi.org/10.1103/PhysRevLett.105.237203

[SAG2014] H. Sagayama, et al., Ferroelectricity driven by charge ordering in the A-site ordered perovskite manganite, SmBaMn2O6, Phys. Rev. B, 90 (24), 241113 (2014); http://dx.doi.org/10.1103/PhysRevB.90.241113

[SCI2004] Ph. Schiau et al. Structural investigation of AgNbO3 phases using x-ray and neutron diffraction, J. Phys.: Condens. Matter 16, 2795 (2004); http://dx.doi.org/10.1088/0953-8984/16/16/004

[SEK1976] T. Sekine et al., Phase equilibria in the system Fe-Fe2O3-Lu2O3 at 1200°C, J. Solid State Chem. 17, 49 (1976); http://dx.doi.org/10.1016/0022-4596(76)90200-0

[SEN2015] M. S. Senn et al., Phys. Rev. Lett. 114, 035701 (2015); Negative Thermal Expansion in Hybrid Improper Ferroelectric Ruddlesden-Popper Perovskites by Symmetry Trapping, http://dx.doi.org/10.1103/PhysRevLett.114.035701

[SHI2016] L.A Shilkina et al. Features of Phase Formation in the Preparation of Bismuth Ferrite. Parinov I., Chang SH., Topolov V. (eds) Advanced Materials. Springer Proceedings in Physics, vol 175. Springer, Cham. (2016); http://dx.doi.org/10.1007/978-3-319-26324-3_6

[SKR2016] L. V. Skripniko et al., LCAO-based theoretical study of PbTiO3 crystal to search for parity and time reversal violating interaction in solids, J. Chem. Phys 145 054115 (2016); http://dx.doi.org/10.1063/1.4959973

[SON2016] S. Song et al., Implementing Room-Temperature Multiferroism by Exploiting Hexagonal-Orthorhombic Morphotropic Phase Coexistence in LuFeO3 Thin Films, Advanced Materials 28, 7430–7435 (2016); http://dx.doi.org/10.1002/adma.201601989

[TAN2006] H. Tanaka et al., Electrostatic potential of ferroelectric PbTiO3: Visualized electron polarization of Pb ion, Phys. Rev. B 74, 172105 (2006). http://dx.doi.org/10.1103/PhysRevB.74.172105

[TAN1983] M. Tanaka et al., Magnetic ordering in Lu2Fe3O7, J. Mag. Mag. Mater. 31, 769 (1983); http://dx.doi.org/10.1016/0304-8853(83)90676-5

[TER2015] N. Terada et al., Ferroelectricity induced by ferriaxial crystal rotation and spin helicity in B-site-ordered double-perovskite multiferroic In2NiMnO6, Phys Rev B 91, 104413 (2015); http://dx.doi.org/10.1103/PhysRevB.91.104413

[TOK2014] Y. Tokura et al, Multiferroics of spin origin, Multiferroics of spin origin, Rep. Prog. Phys. 77 (2014) 076501 (45pp) http://dx.doi.org/10.1088/0034-4885/77/7/076501

[VAL1999] M. Valant and D. Suvorov, New High-Permittivity AgNb1-xTaxO3 Microwave Ceramics: Part II, Dielectric Characteristics, Am. Ceram. Soc. 82, 88−93 (1999); http://dx.doi.org/10.1111/j.1151-2916.1999.tb01727.x

[WAN2013] W. Wang et al., Room-Temperature Multiferroic Hexagonal, LuFeO3 Films, Phys. Rev. Lett. 110, 237601 (2013); http://dx.doi.org/10.1103/PhysRevLett.110.237601

[WU2009] X. B. Wu et al., Study on dielectric and magnetodielectric properties of Lu3Fe5O12Lu3Fe5O12 ceramics, Appl. Phys. Lett. 95, 182903 (2009); http://dx.doi.org/10.1063/1.3259651

[YAS2011] M. Yashima et al., Structure of Ferroelectric Silver Niobate AgNbO3, Chem. Mater. 23, 1643 (2011); http://dx.doi.org/10.1021/cm103389q

[YAS2012] M. Yashima and S. Matsuyama, Origin of the Ferrielectricty and Visible-Light Photocatalytic Activity of Silver Niobate AgNbO3, J. Phys. Chem. C 116, 24902 (2012); http://dx.doi.org/10.1021/jp310589e

[YUA2015] B. Yuan, et al. Structural, magnetic, and dielectric studies of the Aurivillius compounds SrBi5Ti4MnO18 and SrBi5Ti4Mn0.5Co0.5O18, J. Appl. Phys., 117(2), 023907 (2015); http://dx.doi.org/10.1063/1.4905848

[ZHA2007] Y. Zhang et al., Charge-Stripe Order in the Electronic Ferroelectric LuFe2O4, Phys. Rev. Lett. 98, 247602 (2007); http://dx.doi.org/10.1103/PhysRevLett.98.247602

[ZHA2014] C. Zhang et al., Hydrothermal synthesis and multiferroic properties of Y2NiMnO6, RSC Adv. 4, 50969 (2014); http://dx.doi.org/10.1039/c4ra07099b

[ZHA2015] H.J. Zhao et al., Near room-temperature multiferroic materials with tunable ferromagnetic and electrical properties, Nature Commun. 5, 4021 (2015) http://dx.doi.org/10.1038/ncomms5021A

APENDIXES - WORK ORGANIZATION AND EXECUTION

A1 THEMATIC

Table 1 presents a résumé of materials, targeted physics and envisaged nuclear probes.

Table I: Compounds and Targeted Physics

*Legend: **P** = Polarization, **T** = Temperature, **EFG** = Electric Field Gradient, **B**= Hyperfine Magnetic Field*

Compounds	Type	Laboratory	Targeted Physics	Radioactive Probes		People
	morphology	Production, characterization	Local probing of structural and magneto / ferroelectric phase transitions	Specifically produced at ISOLDE	Implanted at RUBION-Bochum BONIS-Bonn	Pos-Doc (PD) PhD Std. (PhDS)
PRIORITY CASES						
$BiFeO_3$	Pellet	CENIDE Essen	***Bi*** site probing of magneto-electric coupling. ^{111m}Cd/Cd and ^{204m}Pb/Pb, crosscheck for electronic relaxation effects upon parent decay of ^{111}In/Cd and ^{204}Bi/Pb @ ***Bi*** site. Information source: ***EFG (T) + B(T)***	^{204}Bi(11.2h)/Pb ^{204m}Pb(67m)/Pb ^{111m}Cd(48m)/Cd	^{181}Hf(42d)/Ta ^{111}In(2.8d)/Cd	1PD
$AgNbO_3$, $AgTaO_3$	Pellet, SC	UDEMAT Essen	***Ag, Ta*** site probing of structural paraelectric, antiferroelectric and ferroelectric transitions. ^{111m}Cd/Cd crosscheck for electronic relaxation effects upon parent decay of ^{111}Ag/Cd and ^{111}In/Cd @ ***Ag*** site. Information source: ***EFG(T) + B(T)***	^{111}Ag(7.4d)/Cd ^{111m}Cd(48m)/Cd	^{181}Hf(42d)/Ta ^{111}In(2.8d)/Cd	1PhDS
$LuFeO_3$, $LuFe_2O_4$, $Lu_3Fe_5O_{12}$	Pellet	CICECO Aveiro	***Lu*** site probing of ferroelectric/magnetic behavior. Information source: ***EFG([Fe],[O],T) + B([Fe],[O],T)***	^{172}Lu(6.7d/Yb	-	1PhDS
$LuMnO_3$	Pellet	CICECO Aveiro	***Lu*** site probing of ferroelectric/magnetic behavior Information source: ***EFG(T) + B(T)***	^{172}Lu(6.7d)/Yb	-	1PD
Ruddlesden Popper: $Ca_3(Mn/Ti)_2O_7$ $Ca_{2-x}Gd_x(Mn/Ti)_2O_7$	Pellet	IFIMUP Porto	***Ca***, ***Gd*** sites probing of uncompensated octahedral rotations and spontaneous Ferroelectricity in layered structures. Information source: ***EFG([Mn],[Ti],x,T)***	^{149}Gd(9.3d)/Eu ^{111m}Cd(48m)/Cd	^{111}In(2.8d)/Cd	1PhDS
TEST CASES						
$CuInP_2S_6$	Pellet, SC	Uzhgorod Univ.; Vilnius University	***In*** site probing of first-order, order-disorder, paraelectric to ferrielectric phase transition. ^{111m}Cd/Cd crosscheck for electronic relaxation effects upon parent decay of ^{111}In/Cd @ ***In*** site. Information source: ***EFG(T)***	^{111m}Cd(48m)/Cd	^{111}In(2.8d)/Cd	1PhDS
ATiO_3, ***A***ZrO_3 ***A*** = Ba, Pb	Pellet; SC	Acad. Sciences Czech Republic; Commercial	Sensitive probing of spontaneous polarization variations at ***A*** site. Information source: ***EFG(P, T) + B(P, T)***	^{111m}Cd(48m)/Cd ^{204m}Pb(67m)/Pb	-	1PD
Ordered double perovskites ***A*** $NiMnO_6$ ***A*** = In, Y, Bi, Gd	Pellet	IFIMUP Porto	Understand the ***A*** site radii variance role on polarization values and switching. Understand the rare-earth ***A*** site substitutions role in short-range magnetic correlations and polar order. ^{111m}Cd/Cd and ^{204m}Pb/Pb, crosscheck for electronic relaxation effects upon parent decay of ^{111}In/Cd and ^{204}Bi/Pb @ ***A*** site. Information source: ***EFG(A,T) + B(A,T)***	^{111m}Cd(48m)/Cd ^{149}Gd(9.3d)/Eu ^{204}Bi(11.2h)/Pb ^{204m}Pb(67m)/Pb	^{111}In(2.8d)/Cd	1PhDS

A2 WORKING WAY:

Sample characterization, non-radioactive techniques

Samples are characterized using techniques available at the home institutes **before** and **after** experiments performed with the radioactive isotopes. Among techniques available within the collaboration, we mention: Characterization X-ray diffraction (powder, high resolution, single crystal), Scanning Electron Microscopy (SEM) with Energy Dispersive X-ray (EDX) analysis, Transmission Electron Microscopy (TEM) and High Resolution TEM with temperature variation (20-300K). Also available are Scanning Probe Microscope (SPM), Atomic-force microscopy (AFM) and Piezoresponse Force Microscopy (PFM) techniques. Rutherford Back Scattering/Channeling (RBS/C) ion beam analysis characterizing micron scaled surface composition and defects on implanted regions is further available.
Magneto-electro characterization is available with Magnetic (SQUID, VSM, ac susceptibility), Dielectric and Electric resistivity measurements (with magnetoresistance).

A3 WORKING WAY:

Radioactive techniques

Isotopes produced at ISOLDE are collected in the general-purpose implantation chamber at the GLM- beam line or at the Small-Implantation-Chamber (SIC chamber) that can fit the GHM- or LA1- beam lines on b. 170. Mounting and dismounting samples at the implantation sample holders is done at the dedicated fume hood in b. 170. Further annealing treatments and PAC experiments are done off-line in the ground floor of building 508, rooms R-004 (furnace room) and R-008 (off-line PAC and Mossbauer laboratory). Once out of the sample holders, after checking of activity, the implanted samples are transported on individual boxes, inside led containers. The samples are "solid" material, consisting self-sustaining pellets, single crystals, or thin films. For annealing treatments under vacuum or gas flow, several furnace systems exist at ISOLDE, which are equipped with traps for fixing volatile elements. If necessary, closed glove boxes exist for handling samples and sample holders during the preparation steps before the measurements.

A 1st step annealing to recover implantation defects is necessary that can be done in parallel using three different tubular furnaces and a rapid thermal annealing system sitting at the furnace room on 508-R-004. Annealing can be done under vacuum, air, Ar, N_2 , He, and a special mixture $[Ar]_{97\%}+ [H_2]_{3\%}$.
Theγ-γ PAC technique is well established at ISOLDE. On building 508-R-008 there are:

- Four 6-Detector PAC spectrometers, ideal to measure polycrystalline / pellet samples.
    - Two 6-Det setups are equipped with furnaces allowing measurements as a function of temperature up to 1173 K under vacuum, air or gas flow. These setups have a load-lock system allowing fast transfer of samples from ambient conditions to the hot spot already set to the measuring temperature.
    - One 6-Det setup is equipped with a closed cycle refrigerator for low temperature measurements down to 10K. This setup has a load-lock system allowing fast transfer of samples from ambient conditions to the cold spot already set to the measuring temperature.
    - One 6-Det setup can be equipped with a special sample holder for orienting single crystals measured at room temperature.
    - Two of the 6-Det PAC spectrometers have high- resolution, high efficiency La(Ce)Br3 and CeBr3 detectors with energy resolution ~3% for 600 keV. The remaining setups have BaF2 detectors. For all setups time resolution, depending on gamma energies range 0.5 – 1.0 ns.

- Two 4-Detector PAC setups, generally used to perform measurements at room temperature dedicated to check recovery of implantation defects after the 1st annealing step, or to perform EFG orientation measurements with single crystals.
    - One of these setups can have an extra furnace mounted or, alternatively, a special closed cycle refrigerator to perform experiments down to 4.5K. Since the cooling time is about 2h after sample insertion, this setup can only be used with isotopes with half-lives greater than few hours.

- Liquid nitrogen dewars are available for fixed temperature measurements on all setups.

Table II: Practical information upon preparing experiments per isotope

Isotope	Samples prepared at	Experiments at ISOLDE	Atoms per collection, per sample (10^{11})	Activity (MBq)	Number of spectra per collection, per sample (approx.)	Acquisition time per spectrum (approx.)
^{111m}Cd (49 m)	ISOLDE	1st annealing	0.3	8		
↓		γ-γ PAC $T_{1/2}$= 85ns, I= 5/2			1	3h
^{111}Cd(stable)						
^{111}In (2.8d)	BONIS RUBION	1st annealing	1	0.28	15 - 25	3h□12h (*)
↓		γ-γ PAC $T_{1/2}$= 85ns, I= 5/2				
^{111}Cd(stable)						
^{111}Ag (7.45 d)	ISOLDE	1st annealing	3 - 5	0.2 - 0.5	5 - 10	1d □1w (*)
↓		γ-γ PAC $T_{1/2}$= 85ns, I= 5/2				
^{111}Cd(stable)						
^{149}Gd (9.3d)	ISOLDE	1st annealing	1.5 - 2.5(***)	0.1 - 0.2	~5	2d □1w (*)(**)
↓		γ-γ PAC $T_{1/2}$= 2450ns, I= 11/2				
^{149}Eu(93.1d)						
^{172}Lu (6.7d)	ISOLDE	1st annealing	2 - 5	0.2 - 0.6	5 - 10	1d □1w (*)
↓		γ-γ PAC $T_{1/2}$= 8.33ns, I=5/2				
^{172}Yb(stable)						
^{181}Hf (42d)	BONIS RUBION	1st annealing	5	0.1	20 - 30	12h – 5d (*)
↓		γ-γ PAC $T_{1/2}$= 10.8ns, I=5/2				
^{181}Ta(stable)						
^{204m}Pb (67m)	ISOLDE	1st annealing	0.15(***)	2.6	1	4h
↓		γ-γ PAC $T_{1/2}$= 265ns, I=4				
^{204}Pb(stable)						
^{204}Bi (11.2h)	ISOLDE	1st annealing	1(***)	1.7	2 - 5	3-6
↓		γ-γ PAC $T_{1/2}$= 265ns, I=4				
^{204}Pb(stable)						

(*) Measuring time increases with the decrease of activity;
(**) Probing PAC state with a big half-life of 2.45μs. It requires more time to get statistics within the first 500 – 1000 ns of analysis where most of the fields should be resolved.
(***) The True to Chance (T/C) coincidence ratio on a PAC experiment is proportional to the parent's nuclei half-life divided by the PAC measuring state half-life and the number of radioactive nuclei. When the PAC state half-life is too big (typically greater than 100 ns) that sets a significant limit on the number of radioactive nuclei per experiment, per sample. T/C should never be less than 1, to avoid that the data becomes dominated by uncorrelated chance coincidences. This is particularly critical on short lived isotopes.

A3 WORKING WAY:

OFF-LINE experiments with short lived isotopes

We describe the *Cycle of Preparation and Measurements* (CPM) required to run PAC experiments OFF-LINE with isotopes of few tens of minutes' half-life produced at ISOLDE. After the CPM description, a block diagram is presented visualizing the multi-step procedure necessary to accomplish such type of experiments.

1- A typical CPM consists of a 4-hour periodic schedule handling multi-sample parallel experiments.

2- The CPM starts by mounting 4 samples at the sample holder (10-15 min), followed by the insertion at the GLM-SSP collection chamber (b.170 GLM-beam line) when vacuum pumping can start (20 min).

3- The 4 samples are then sequentially implanted. Due to the short half-life (48min ^{111m}Cd), depending on beam yields, this step can take 20 – 40 min (max).

4- Removal of the sample holder from the GLM SSP chamber. At the fume-hood on b. 170 we proceed to the removal and separation of samples by individual small plastic boxes, which are then merged on Lead containers and transported to building 508 – furnace room.

5- A first annealing step is performed to recover implantation defects at the tubular furnaces. 4 different furnaces are dedicated to each sample annealing specifications. Generally, a 10 – 20 min annealing step is performed under required atmosphere (air, N_2, Ar, He, vacuum).

6- Then the samples are mounted at dedicated PAC sample holders, fitting each one a specific PAC spectrometer. Fast load-lock transfer systems allow the samples to be placed in situ at the desired measuring temperature to fasten the start of the measurement. At this point about 1h – 1h 20min has vanished since the start of collections at the GLM-SSP chamber.

7- With a half-life of 48min (^{111m}Cd), 3 hours are required to get a measurement with essential statistics.

8- The duty cycle of the remaining two PAC spectrometers follows the same procedure, starting at point 1, but *out-of-phase* by 2 hours with the current 4-batch sample's CPM.

9- About one hour before the running CPM ends, a new cycle starts at point 1.

NOTE 1: The different PAC setups run in parallel. Two of these are equipped with furnaces to perform measurements as a function of temperature and two others with closed cycle refrigerators for low temperature measurements. The two remaining setups perform measurements at room temperature or at liquid nitrogen.

NOTE 2: Each type of material SHOULD be measured on the SAME spectrometer to allow systematic data to be easily compared. In this way we avoid systematic deviations from different solid angles, efficiencies and time resolution that affects the amplitude of the R(t) function and the determination of absolute fractions of nuclei interacting with different environments. Every machine is calibrated to the maximum observable amplitude and time resolution before experiments start.

NOTE 3: In the case of short lived isotopes every point taken as a function of, e.g., temperature, requires a full new CPM on a new sample piece from the same batch of material. Sample's (areal) size can vary from a couple of mm^2 to several mm^2 (max 5x5 mm^2) with thicknesses not greater than 1 mm and not smaller than 0.1 mm … depending on sample's robustness.

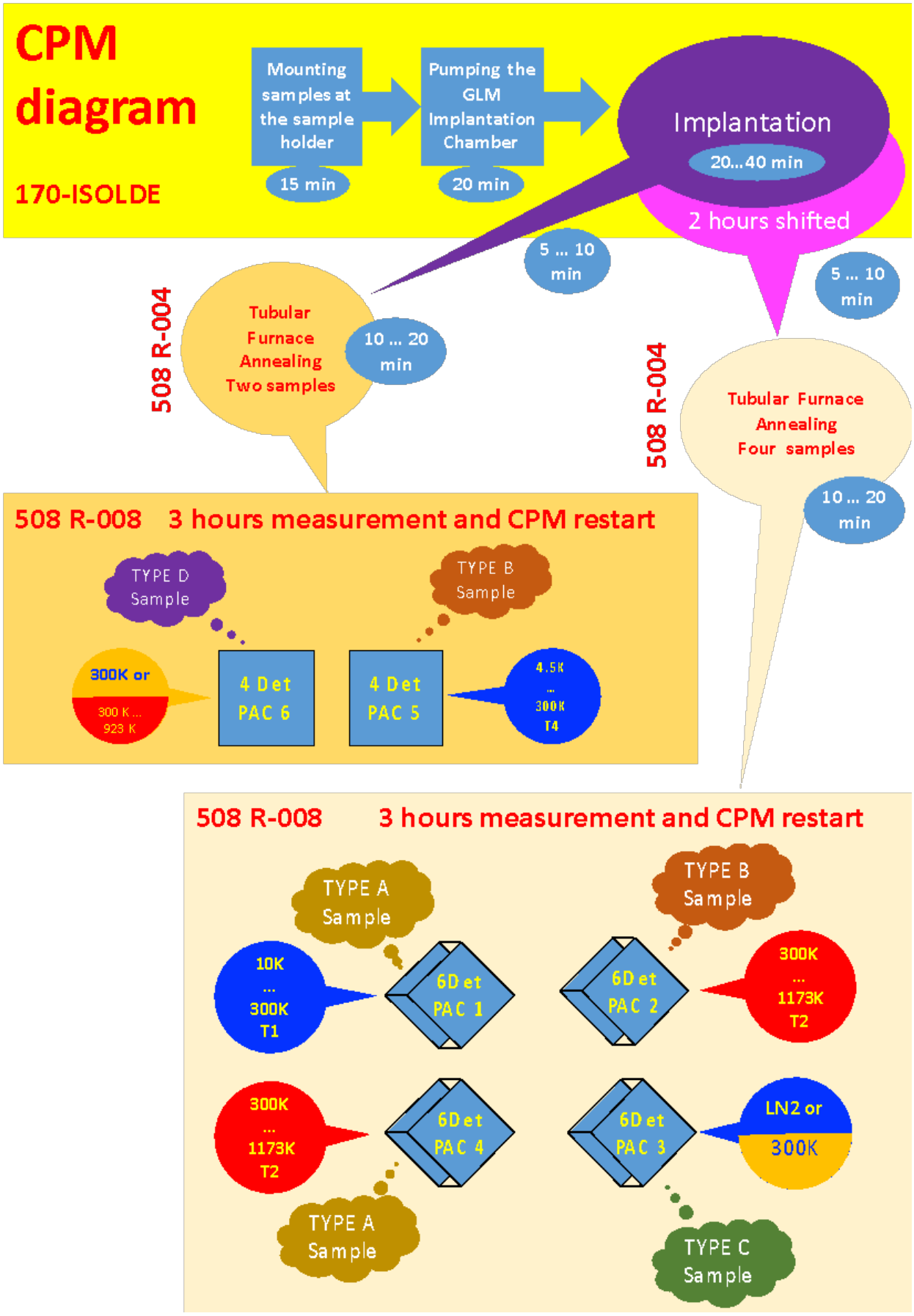
CPM diagram
170-ISOLDE
Mounting samples at the sample holder
15 min
Pumping the GLM Implantation Chamber
20 min
Implantation
20...40 min
2 hours shifted
5 ... 10 min
5 ... 10 min
508 R-004
Tubular Furnace Annealing Two samples
10 ... 20 min
508 R-004
Tubular Furnace Annealing Four samples
10 ... 20 min
508 R-008 3 hours measurement and CPM restart
TYPE D Sample
TYPE B Sample
300K or
300 K ... 923 K
4 Det PAC 6
4 Det PAC 5
4.5K ... 300K T4
508 R-008 3 hours measurement and CPM restart
TYPE A Sample
TYPE B Sample
10K ... 300K T1
6Det PAC 1
6Det PAC 2
300K ... 1173K T2
300K ... 1173K T2
6Det PAC 4
6Det PAC 3
LN2 or 300K
TYPE A Sample
TYPE C Sample

A4 Description of the proposed experiment

The experimental setup comprises:
(name the fixed-ISOLDE installations, as well as flexible elements of the experiment)

Part of the Choose an item.	Availability	Design and manufacturing
SSP-chamber @ GLM	☐ Existing	☐ To be used without any modification
Existing equipment on the solid state labs in building 115 - 6 detector PAC standard setups - annealing furnaces - glove boxes	☐ Existing	☐ To be used without any modification ☐ To be modified
	☐ New	☐ Standard equipment supplied by a manufacturer ☐ CERN/collaboration responsible for the design and/or manufacturing

HAZARDS GENERATED BY THE EXPERIMENT

(if using fixed installation) Hazards named in the document relevant for the fixed SSP-GLM chamber and building 508 installations.

Additional hazards:

Hazards			
	SSP-GLM	*Building 508-R-04,08*	*[Part 3 of the experiment/equipment]*
Thermodynamic and fluidic			
Pressure	[pressure][Bar], [volume][l]		
Vacuum	10-6 mbar at SSP chamber 10 during collections		
Temperature			
Heat transfer	-		
Thermal properties of materials	-		
Cryogenic fluid		Liquid nitrogen, 1 Bar, few litres used during the PAC measurements on appropriate glass dewar.	
Electrical and electromagnetic			
Electricity	[voltage] [V], [current][A]		
Static electricity			
Magnetic field	[magnetic field] [T]		
Batteries	☐		
Capacitors	☐		
Ionizing radiation			
Target material	[material]		
Beam particle type (e, p, ions, etc)			

Beam intensity			
Beam energy			
Cooling liquids	[liquid]		
Gases	[gas]		
Calibration sources:	☐		
• Open source	☐ Produced at ISOLDE: 111mCd (49 m) 111Ag (7.45 d) 149Gd (9.3d) 172Lu (6.7d) 204mPb (67m) 204Bi (11.2h) Produced elsewhere: 181Hf (42d) 111In(2.8d)	Sources to be measured at 508	
• Sealed source	☐	22Na sources provided by RP services at CERN, used at 508	
• Isotope	111mCd (49 m) 111Ag (7.45 d) 149Gd (9.3d) 172Lu (6.7d) 204mPb (67m) 204Bi (11.2h) 181Hf (42d) 111In(2.8d)		
• Activity (per sample)	111mCd (49 m) 8MBq 111Ag (7.45 d) 0.2 - 0.5MBq 149Gd (9.3d) 0.1 - 0.2MBq 172Lu (6.7d) 0.2 - 0.6MBq 204mPb (67m) 2.6MBq 204Bi (11.2h) 1.7MBq 181Hf (42d) 0.1MBq 111In(2.8d) 0.3MBq		
Use of activated material:	none		
• Description	☐		
• Dose rate on contact and in 10 cm distance	[dose][mSV]		
• Isotope			
• Activity			
Non-ionizing radiation			
Laser	none		
UV light	none		
Microwaves (300MHz-30 GHz)	none		
Radiofrequency (1-300MHz)	none		
Chemical			
Toxic			
Harmful			
CMR (carcinogens, mutagens and substances toxic to reproduction)	[chemical agent], [quantity]		
Corrosive	[chemical agent], [quantity]		
Irritant	[chemical agent], [quantity]		
Flammable	[chemical agent], [quantity]		

Oxidizing	[chemical agent], [quantity]		
Explosiveness	[chemical agent], [quantity]		
Asphyxiant	[chemical agent], [quantity]		
Dangerous for the environment			
Mechanical			
Physical impact or mechanical energy (moving parts)	[none]		
Mechanical properties (Sharp, rough, slippery)	[none]		
Vibration	[none]		
Vehicles and Means of Transport	[none]		
Noise			
Frequency	[frequency],[Hz] Ambient noise at the ISOLDE Hall, building 170		
Intensity	Ambient noise at the ISOLDE Hall, building 170		
Physical			
Confined spaces	[none]		
High workplaces	[none]		
Access to high workplaces	[none]		
Obstructions in passageways	[none]		
Manual handling	All samples and sample holders are manually handled either by long tweezers to insert and extract the sample holder into and out of the SSP implantation chamber at GLM, or when manipulating the samples and sample holders inside glove boxes or fume houses on building 508	All samples and sample holders are manually handled either by long tweezers to insert and extract the sample holder into and out of the SSP implantation chamber at GLM, or when manipulating the samples and sample holders inside glove boxes or fume houses on building 508	
Poor ergonomics	[none]		

0.1 Hazard identification

3.2 Average electrical power requirements (excluding fixed ISOLDE-installation mentioned above): *(make a rough estimate of the total power consumption of the additional equipment used in the experiment)*
There is no additional equipment with relevant power consumption on these small-scale experiments.